



Comparative experimental and modelling study of the thermal and thermo-mechanical properties of LLDPE/wax blends

Mafereka F. T. Mosoabisane¹ · Adriaan S. Luyt² · Cornelia G. C. E. van Sittert³

Received: 13 January 2022 / Accepted: 13 June 2022 / Published online: 25 June 2022
© The Author(s) 2022

Abstract

The interactions and morphology of molecules in a polymer blend influence the physical properties of the blend. However, little is known about the influence of molecular interaction and morphology on the thermal and mechanical properties of LLDPE/wax blends. Although cooling rate can be used to investigate blends' thermal and mechanical properties, it is inadequate to determine interactions between the molecules in the LLDPE/wax blends. However, since the morphology is related to the thermal and mechanical properties of polymer blends and could be related to the cooling rate, LLDPE/wax samples prepared by melt mixing were cooled at different rates. The thermal and mechanical properties of the LLDPE/wax blends were modelled through molecular dynamic simulations. The modelled transitions were compared to experimentally determined mechanical relaxations of LLDPE/wax blends to investigate the effect of wax addition on the blend crystallinity. The crystallization behaviour of the blends was studied by differential scanning calorimetry, dynamic mechanical behaviour by dynamic mechanical analysis, and differences in crystallinity by X-ray diffraction. There were no significant differences between the results for the slow- and quench-cooled samples, confirming the rapid crystallization of both the LLDPE and the wax. Experiments and molecular dynamics simulations confirmed the cocrystallization of wax with LLDPE.

Keywords LLDPE/wax blends · Molecular simulation · Thermal properties · Cocrystallization

Introduction

Many polymer scientists used either experiments or computational models to investigate the relationships between the interactions of molecules and their morphology on macro and micro scales and their influence on various properties of the polymer [1, 2]. These relationships are linked to the molecular arrangements and interactions of the polymeric structures at an atomic level. These interactions could be between the same type of molecules or between different types of molecules within polymer mixtures (blends). The thermal and mechanical properties of polymers are strongly

influenced by their morphology, degree of crystallinity and crystal structure [3]. Therefore, there is a correlation between polymer properties, molecular arrangement, and surface morphology.

Polymer morphology can be predicted by looking at the polymer relaxation dynamics when the polymer is either heated to or cooled from a melt. Instead of using expensive synthetic routes, the physical mixing of polymers to create new materials, such as blends or composites with specific properties, is used. Examples of such materials are blends prepared through melt blending of polyethylene(s) with other polymers or wax [1, 4, 5]. The properties of blends depend on the mixing method (for example, melt mixing or extrusion), their weight per cent in the total system, and how they are cooled from a melt.

The polyethylene molecular structure is controlled by the degree of crystallinity, branching and density. Therefore, different classes of polyethylenes are synthesized for use in specific applications. Semi-crystalline linear low-density polyethylene (LLDPE) copolymer, synthesized from ethylene and alpha-olefins such as 1-butene, 1-hexene and 1-octene, is of great technological importance [6]. The effects of

✉ Adriaan S. Luyt
aluyt@qu.edu.qa

¹ Department of Chemistry, University of the Free State (Qwaqwa Campus), Phuthaditjhaba, South Africa

² Center for Advanced Materials, Qatar University, Doha, Qatar

³ Laboratory for Applied Molecular Modelling, Research Focus Area: Chemical Resource Beneficiation, North-West University, Potchefstroom, South Africa

branching (branch length and content) on the crystallinity of LLDPE have been studied with regard to crystallization and melting temperatures, crystal size and shape, and cooling rate and molar mass [6–9]. The results obtained in these studies are well explained in terms of different variables related to the crystalline structure of the LLDPE.

Although polymer scientists mixed existing polyethylenes to create new materials and characterize them in terms of their physical properties, the emerging challenge is to fully describe these properties in terms of their morphologies. This challenge is because material properties, like morphology and crystallinity, get more complex to solve when the polymers interact [10]. The morphologies of polyethylene and its blends have been well researched, especially concerning their crystallinities [11–13]. Blends based on polyethylenes have different morphologies, and the properties depend upon the blend composition and the crystallinities of the blend components. Different research groups studied a wide range of properties affected by the crystallization mechanism in polyethylene/polyethylene and/or polyethylene/wax blends [5, 13, 14].

For example, the role of crystallization conditions on the morphology of polyethylene blends was studied [14, 15]. Simple and sophisticated experiments under isothermal and non-isothermal conditions at cooling rates applied in industrial processes [16], were also used to study the crystallinity of polyethylene/wax blends. Different processing methods also influence the structure of the resulting new materials and their morphologies [17]. Additionally, the morphology of some polymer blends may be affected by crystallizing the prepared samples at different cooling rates (fast and slow cooling). The materials were crystallized from the melt under different conditions in previous studies. The crystallized materials were then analyzed using dynamic mechanical analysis (DMA) [5] and differential scanning calorimetry (DSC) as analytical tools to study their relaxation transitions [18].

Relaxation dynamics is often used to investigate the crystallinity of polyethylene because polyethylene molecules undergo different structural changes when they are cooled from a solution or a melt. It was reported that polyethylene undergoes three mechanical relaxations during the cooling or heating process, namely γ -, β -, and α -relaxation [19]. These relaxations describe polyethylene's structural changes during crystallization and explain various properties of the different types of polyethylene [19, 20]. For instance, to predict the deformation process of the amorphous part in polyethylene, a physical model was applied to study γ -relaxation [20]. Therefore, by analyzing both the dynamic and mechanical behaviour of the amorphous phase, it was confirmed that the crystallites act as physical ties between the amorphous chains. Thermal and dynamic mechanical properties were investigated to determine the influence of

branch concentration on the γ -, β -, and α -relaxations in an ethylene/1-octene copolyethylene [21]. To summarize, there is a relationship between the structure (morphology) and the physical properties of a semicrystalline polyethylene that has been grown from solution or melt [3].

Several theoretical models have been developed to study the morphology of polymer crystals in terms of chain folding and molecular mobility [22, 23]. However, computer simulations became an important tool to complement the theoretical models due to a lack of suitable experiments to fully test the proposed theoretical models [10]. Some of these computer simulations were validated by comparison with experimental data [24, 25]. It implies that computer simulations could be sufficient when experiments are difficult to perform. For example, the study of the crystallization dynamics of polymers, which commonly occurs too far from equilibrium, is difficult through experimental analysis [11]. The crystallization dynamics of polyethylene from the melt was studied using atomistic molecular dynamic simulations. The mechanism of chain folded lamellae and the growth and cold crystallization of long polyethylene crystals at temperatures around the glass transition temperature were investigated with a united atomistic model [12]. The united atomistic model predicted small granular crystallites during cold crystallization and fast thickening of the folded chain lamellae. In another similar study, homogeneous crystal nucleation of polyethylene under supercooling was studied to characterize the crystal surface topology based on loops and tails.

However, molecular dynamics simulation can complement experimental studies to solve the crystallinity and morphology of polyethylenes and their blends [25, 26]. These simulations were successfully used to investigate melt dynamics and phase transitions of polyethylene [2]. Since polyethylene morphology is generally described in terms of crystalline and amorphous phases, molecular dynamics and experiments were able to show that molecules form entanglements in the melt and folds in the crystalline state. The degree of crystallinity is controlled by the kinds of monomers, tacticity, branching and the type of blend and blend ratios used [27]. Both experiments and computational models successfully described the polyethylene crystallinity by looking at chain movements in the molten and solid states [28].

In this study, LLDPE/wax blends were investigated. Because of its highly crystalline structure, paraffin wax is a good candidate material to be blended with polyethylene, particularly with the versatile LLDPE, to form efficient phase change materials [29]. Medium soft paraffin wax can be cocrystallized with LLDPE when the physically mixed blends are cooled from the melt or act as a plasticizer by decreasing the crystallization and melting temperatures of LLDPE [16]. The molecular mechanistic

pathways in which cocrystallization and plasticization occur are difficult to determine through experiments [30]. Blend compositions and chain lengths have been used as a theoretical model to study the crystallization of the polymer blends in the context of a kinetics description of polymer crystal growth [31, 32].

A possible way to determine the molecular mechanistic pathways in which cocrystallization and plasticization of the LLDPE/wax blends occur is to use atomistic molecular dynamic simulations. According to the authors' knowledge, no reports have been published on studies done on LLDPE/wax blends using atomistic molecular dynamic simulations. The chain movements in the melt of many polymer blends were investigated by simulating the heating and cooling processes [30]. The variables such as density, specific volume and thermal expansion were used to study a blend's relaxation mechanism through molecular dynamics simulation to establish the structural, thermal or dynamic properties [33, 34].

In this study, atomistic molecular dynamic simulation was combined with DMA, DSC and XRD experiments to investigate the effect of wax content on the LLDPE relaxation dynamics. The crystallinity of the neat wax, LLDPE and their blends were investigated by studying the thermal history obtained experimentally for all the materials used. The relationship between the theoretical and computational models of systems created using short wax and long LLDPE chains were established by predicting and monitoring all the materials' glass transition temperatures.

Materials and methods

Materials

The blends were prepared using LLDPE purchased from Sasol Polymers (a division of Sasol Chemical Industries, Johannesburg, South Africa). The copolymer comprises of 2.1% hexene branches with a melt flow index (MFI) of 1.0 g/10 min (190 °C, 2.16 kg) (ASTM D1238), with an average molecular weight of 191,600 g mol⁻¹, melting temperature of 124 °C and a density of 0.924 g cm⁻³. Medium soft paraffin wax (M3 wax), referred to as 'wax' in the rest of the study, was obtained from Sasol Wax (a division of Sasol Chemical Industries, Johannesburg, South Africa). It consists of 99% straight aliphatic hydrocarbons and a few branches with the formula C_nH_{2n+2}. Its carbon distribution ranges from C15 to C78. It has a density of 0.9 g cm⁻³, melts in a 40–60 °C temperature range, and has an average molecular weight of 440 g mol⁻¹.

Sample preparation

A Brabender Plastograph (Brabender® GmbH & Co., Germany) with a 50 mL internal mixer was used to melt-mix all the samples. The samples were mixed at 170 °C at a speed of 30 rpm for 15 min. The blends were prepared by mixing the pure LLDPE and M3 wax according to the mass ratios shown in Table 1. The mixed samples were melt-pressed under a pressure of 50 kPa for 5 min at 170 °C using a hydraulic hot press. Two sets of samples were prepared. One set of samples was isothermally cooled at room temperature (slow-cooled) for 10–15 min. The other set of samples were quench-cooled in liquid nitrogen for about 10 min. Neat LLDPE and neat wax were treated in the same way.

Determination of thermal and mechanical properties of LLDPE/wax blends

DSC experiments were performed using a PerkinElmer DSC6000 differential scanning calorimeter (PerkinElmer, Waltham, Massachusetts, U.S.A) under a nitrogen flow of 20 ml min⁻¹. Between 5 and 10 mg of each sample was heated from -50 to 160 °C at a rate of 10 °C min⁻¹, cooled to -50 °C at the same rate, and again heated to 160 °C at the same rate. Three analyses were done for each sample. The enthalpies determined from the peak areas were used to indicate the crystallinity of each melting fraction.

The storage and loss moduli (E' and E'') as functions of temperature were determined in a Perkin Elmer Diamond DMA dynamic mechanical analyzer (PerkinElmer, Waltham, Massachusetts, U.S.A.). The analyses were done in bending mode at a frequency of 1 Hz and a heating rate of 3 °C min⁻¹ under a nitrogen atmosphere. LLDPE and the blend samples were heated from -130 to 130 °C. The samples were 50 mm long, 12.6 mm wide, and 1.3 mm thick.

The XRD analysis of LLDPE and the blends were done on an Empyrean X-ray diffractometer. The instrument used a crystal copper anode and K_α radiation in the angular scan range of 2θ = 5–90° with a 40 mA current and 45 kV operating voltage. The instrument applied a continuous scan to

Table 1 Mass ratios of both the slow- and quench-cooled samples

Sample	Mass ratio (w/w)
Neat LLDPE	100
LLDPE/wax	95/5
	90/10
	80/20
	70/30
	60/40
Neat wax	100

the samples. The areas under the amorphous and crystalline regions were determined in arbitrary units.

Molecular simulation methods

Materials Studio (MS) 2018 software [35] from BIOVA through the Centre for High Performance Computing (CHPC) [36] was used to do calculations. Monomers of LLDPE and wax were geometrically optimized using the density functional theory (DFT) [37] module DMol³ in MS. The Forcite molecular mechanics (MM) module, also known as the force fields, in MS was used to simulate the polymer molecules and blends.

Monomer models

As mentioned in the introduction, LLDPE is synthesized from two monomers, namely ethylene and α -olefins: 1-butene, 1-hexene, 1-octene. For this work, only 1-hexene was selected to create the LLDPE molecules. The ethylene and 1-hexene were drawn manually in MS Visualizer [35] and geometrically optimized using DMol³ in MS [37, 38]. Geometric optimization was done using the generalized gradient approximation functional of Perdew and Wang (GGA-PW91) [39, 40] with a double numeric polarized basis set with diffusion (DNP+). The DNP+ basis set was chosen because the polymerization occurs according to a free radical mechanism [40, 41]. Additionally, the basis set performs well against most experimental and analytical basis sets at less simulation time [42].

The following settings were used during the geometry optimization of the monomers: quality of optimization was set to medium, the threshold for the maximum change in energy of 2.0×10^{-5} Hartree (in the Hartree wave function), a maximum force of $0.004 \text{ Hartree } \text{\AA}^{-1}$, number of iterations 50, maximum step size of 0.3 \AA in length between any Cartesian coordinates (maximum allowed length in search of Cartesian coordinates), and 0.005 \AA displacement between points. No symmetry was selected, unrestricted spin state (triplet multiplicity) and charge of zero. The following settings were used in the electronic setup: integration accuracy level set to medium, self-consistent field (SCF) tolerance was 1.0×10^{-5} , 50 SCF cycles maximum, multipolar expansion (hexadecapole) with a global orbital cut-off scheme and smearing of 0.005, all electron core treatment, and a medium orbital cut-off quality was used. Monomer optimization calculations were run in the absence of a solvent.

Construction and optimization of single LLDPE chains

The optimized ethylene and 1-hexene structures were used to construct many single LLDPE polymer chains using the random copolymer build function of MS. Chains with

a length from 10 to 500 (20 to 1000 backbone carbons) with branches, randomly distributed along the backbone, of different content (1-hexene) were built using forced concentrations [43]. All the LLDPE polymer chains, with varying lengths and branch content, were geometrically optimized using the Forcite module with the condensed phase optimized molecular potentials for atomistic simulation studies (COMPASS) force field [44]. COMPASS is an ab initio force field that is consistently parameterized for big molecules, such as polymers in a condensed state [44, 45]. A force field for all-atom simulations of small inorganic molecules, organic molecules, and polymers was produced by ab initio and empirical parametrization techniques [46]. A large number of valence parameters were derived from quantum mechanical calculations of small molecules, and the new Van der Waals parameters were derived by conducting MD simulations of molecular liquids and then compared to other forces like a consistent force field (CFF) if there was no data available for certain new polymers tested by COMPASS. The reliability and validity of COMPASS have been confirmed by fitting data to the experimentally determined properties of large molecules, liquids and crystals. The type II COMPASS has been extended to cover polymers and drug-like molecules without deviation from the original parameters [45]. Therefore, COMPASS is the best choice to optimize LLDPE and its blends. Geometry optimization was done with the Quasi-Newton algorithm because it minimizes structures fast and converges quickly. The convergence tolerance setup was as follows: Quality of minimization was customized with a maximum energy of $0.001 \text{ kcal mol}^{-1}$ and force of $0.5 \text{ kcal mol}^{-1} \text{ \AA}^{-1}$, and the different maximum iterations between points were limited to 0.005 \AA . The contribution of charges in chains was energy minimized by the Gasteiger original within 50 maximum iterations for a convergence limit of $2.0 \times 10^{-5} \text{ kcal mol}^{-1}$.

Cubic simulation boxes, often called periodic systems, were created with the Amorphous Cell module in Materials Studio. All the LLDPE were added to the periodic cells through the technique described by Theodorou and Suter [58] (Fig. 1). The calculation option in the Amorphous Cell module was chosen over the construction (legacy) option because it allows for a minimum of one chain per periodic system, and the construction process was short. The torsion angles were calculated during construction while optimizing the chains without relaxing the lattice parameters. A quasi-Newton algorithm was used to a convergence energy level of $0.00002 \text{ kcal mol}^{-1}$ for smaller molecules and $0.001 \text{ kcal mol}^{-1}$ for large molecules. The energy calculation setup for the cells was as follows: COMPASS force field, original Gasteiger (Gast_original1.0) method for calculating charges, Ewald method for electrostatic summation, and van der Waals energy calculation.

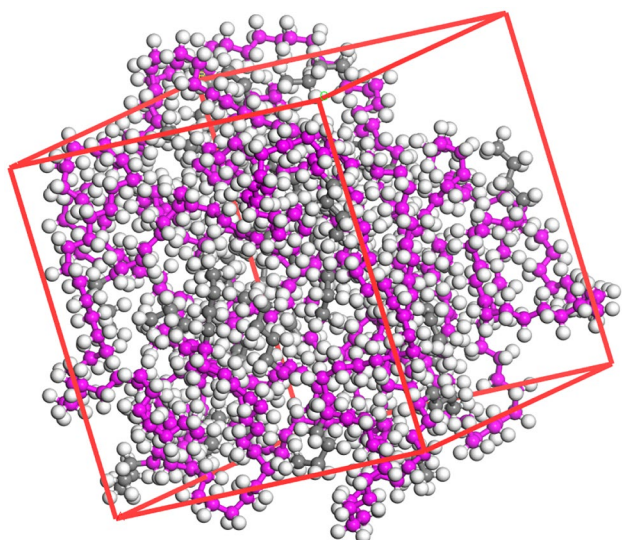


Fig. 1 Amorphous cell of a long LLDPE (520 carbons and 70 branches) single chain after geometric and dynamics optimization at 500 K (purple atoms represent the backbone carbons, grey atoms the carbon branches and white atoms the hydrogens)

One molecular chain per unit cell was constructed for long LLDPE chains (520 carbons in the backbone and 70 branches). This construction was followed by relaxation of the molecule inside the unit cell using an initial NVT and NPT MD ensemble to equilibrate (relax) the polymer chain in the unit cell. A similar process was followed when a unit cell contained more than one molecule, short-chains (branches per 100 carbons in the backbone) and wax molecules to investigate the effect of the number of molecules per unit cell in terms of density. All MD simulation studies were run in the bulk state, without a solvent.

The LLDPE chains in the unit cell were relaxed further by annealing the system from 150 to 450 K and back to 150 K with a heating ramp of 10 K min⁻¹ for 20 cycles.

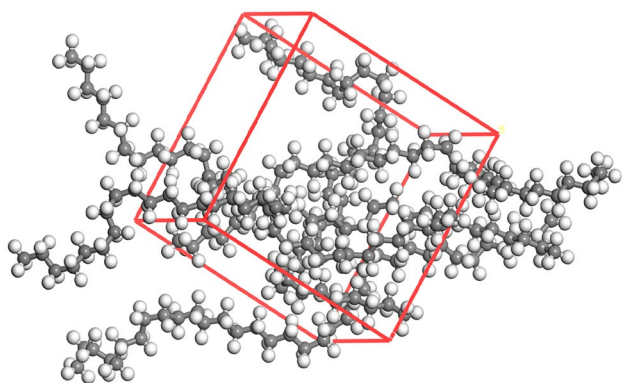


Fig. 2 Amorphous cell of five wax chains after being cooled to 160 K (grey atoms represent the carbons and white atoms the hydrogens)

This treatment of the unit cell was first done with NVT followed by NPT MD [48]. Torsions were calculated automatically at 0.25 radii of Van der Waals forces and loading steps of 1000 ps. The Quasi-Newton method was employed for 1000 ps with a maximum of 50 iterations within the convergence limit of 5.0×10^{-6} kcal mol⁻¹. The partial charge of atoms was estimated using the charge equilibrium method called Gasteiger. The electrostatic energy was calculated by the Ewald summation method at an accuracy level of 0.0001 kcal mol⁻¹. The atom-based summation was adopted for Van der Waals interaction with a cut-off distance of 15.5 Å. After the 20-cycle annealing, a 1000 ps NVT MD simulation at 298 K was carried out, followed by NPT MD, first at 298 K and then at 500 K.

Construction and optimization of wax

The ethylene monomer from the database of MS was used to construct the wax chains. The constructed wax chains with different lengths (C₂₀H₂₂ – C₄₄H₄₆) were geometrically optimized using the Forcite module with the COMPASS force field [44]. Geometry optimization was done with the Quasi-Newton algorithm because the energy convergence is fast and good for short-chain polyethylenes. Periodic wax models (Fig. 2), needed for MD simulations, were created using the Amorphous Cell module in MS. The periodic systems were relaxed with the canonical constant number, volume and temperature (NVT) ensemble MD simulation, followed by an isothermal–isobaric (constant number, pressure and temperature) (NPT) ensemble MD simulation at 298 K for 1000 ps.

Simulation of thermo-mechanical properties of LLDPE/wax blends

The LLDPE polymer and wax models were constructed based on the technique described by Theodorou and Suter [47]. For this construction, cubic simulation boxes, also called periodic systems or unit cells containing LLDPE and wax chains, were constructed using the Amorphous Cell module in MS [35]. The unit cells contained different ratios of long LLDPE chains (520 carbons in the backbone and 70 branches) or short LLDPE chains (100 carbons and 1 branch), and wax (36 carbons long with no branches), to make the desired blend systems. One such a blend system model (long 70/30 w/w LLDPE/wax) is shown in Fig. 3. In the Amorphous Cell module, two options for construction are available, namely cell calculation and construction legacy. The cell calculation was chosen over the construction legacy because it allows for a shorter construction process time (less simulation time) than the construction legacy. The setup was as follows: cubic lattice with an initial density of 0.924 g cm⁻³ for LLDPE and 0.900 g cm⁻³ for wax

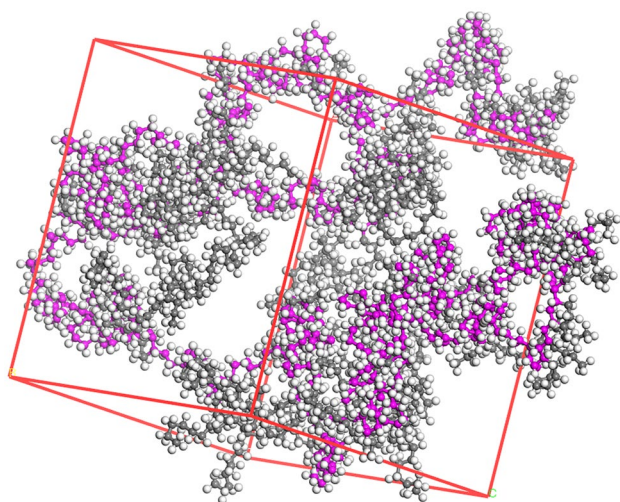


Fig. 3 Amorphous cell of the long 70/30 w/w LLDPE/wax after construction (in the LLDPE molecules, the purple atoms represent the backbone carbons, the grey atoms the carbon branches, and the white atoms the hydrogens; in the wax molecules, the backbone carbons are represented by grey atoms and the hydrogens by white atoms)

(which were the actual densities of the materials used in the laboratory experiments). Torsions were calculated during construction while optimizing the chains but not the lattice parameters. A Quasi-Newton algorithm was used to a convergence energy level of $0.00002 \text{ kcal mol}^{-1}$ for smaller molecules and $0.001 \text{ kcal mol}^{-1}$ for large molecules. The energy calculation setup was as follows: COMPASS was chosen as the force field, charges were calculated by the Gasteiger method, Ewald was used as the electrostatic summation method, and atom-based Van der Waals interactions were used.

Supercells with different numbers of atoms were created and minimized with NPT MD to find the density of the models. These models were then further relaxed. Supercell construction was only possible for short-chain LLDPEs and wax

models. For long LLDPE chains, the computational costs were too high. Supercells (extending in all three dimensions) were constructed using the final stable unit cell after the NVT MD simulations to create the supercells with 27-unit cells. A further NPT MD equilibration was done on the created supercells by following the same settings as the single unit cell.

Molecular dynamics was repeated with the NPT ensemble at different temperatures starting from 500 to 100 K (at 25 K intervals) for 1000 ps without changing any settings in the structural equilibration. In order to compare the models with the experimental results, the blend systems had composition ratios as follows: 95/5 w/w, 90/10 w/w, 80/20 w/w, 70/30 w/w, and 60/40 w/w LLDPE/wax (Table 2). When all the MD runs for all the molecules were finished, the glass transition temperature (T_g) of all the molecules was determined from the various thermodynamic properties obtained. The two properties used to determine T_g were the change in density and volume as a function of temperature [30, 34].

Results and discussion

Thermal properties of LLDPE/wax blends

Figure 4 shows the DSC first heating curves of neat LLDPE, neat wax and their blends. Table 3 shows the observed melting enthalpies (ΔH_w^{ob-sc} , ΔH_w^{ob-qc} , ΔH_L^{ob-sc} , ΔH_L^{ob-qc}), calculated directly from the melting peak areas in the respective DSC curves, for the wax and LLDPE fractions in the blends. It also shows the normalised melting enthalpies (ΔH_w^{n-sc} , ΔH_w^{n-qc} , ΔH_L^{n-sc} , ΔH_L^{n-qc}), calculated by dividing the observed melting enthalpy values by the weight fractions of respectively wax and LLDPE in a particular blend. If the normalised melting enthalpy of, for example, wax is smaller than the observed melting enthalpy of neat wax, a smaller amount of wax crystallized separately in the blend, which indicates that some wax has probably cocrystallized

Table 2 Modelled sizes of the neat materials and their respective blends

Sample	Short LLDPE chains			Long LLDPE chains		
	Cell size (Å)	LLDPE chains	Wax chains	Cell size (Å)	LLDPE chains	Wax chains
Neat LLDPE	29.02	10	0	25.09	1	0
95/5 w/w LLDPE/wax	32.43	13	2	25.68	1	1
90/10 w/w LLDPE/wax	29.28	9	3	26.04	1	2
80/20 w/w LLDPE/wax	26.49	6	4	26.89	1	4
70/30 w/w LLDPE/wax	26.19	5	6	41.16	2	15
60/40 w/w LLDPE/wax	27.47	5	9	44.01	2	24
50/50 w/w LLDPE/wax	24.58	3	8	N/A	N/A	N/A
Neat wax	16.72	0	5	16.72	0	5

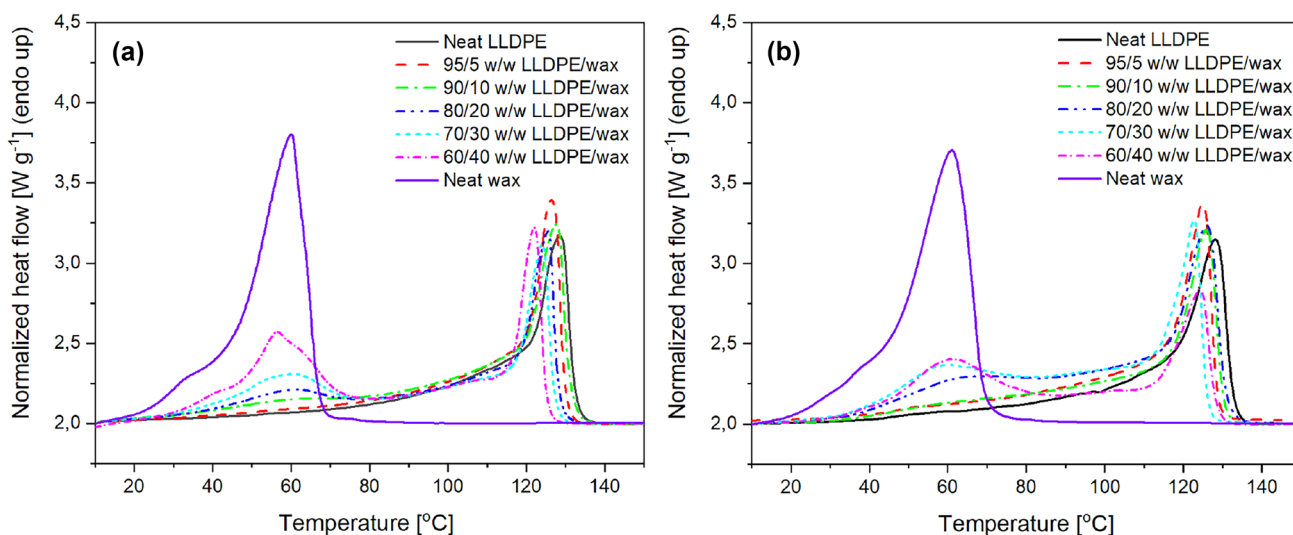


Fig. 4 DSC first heating curves of (a) slow-cooled and (b) quench-cooled neat LLDPE, neat wax and various LLDPE/wax blends

with the LLDPE. This cocrystallization will be confirmed if the normalised melting enthalpy of the LLDPE in the same blend is larger than the observed melting enthalpy of neat LLDPE. After cooling at room temperature, the neat wax shows a melting enthalpy of 154.5 J g^{-1} (Table 3). If all the wax in the blends crystallized separately from the LLDPE, the ΔH_w^{n-sc} values for the melting of wax in the blends should have been very close to the melting enthalpy of neat wax. However, it is clear from Table 3 that these values are significantly smaller than 154.5 J g^{-1} , which indicates that a significant part of the wax is probably cocrystallized with the LLDPE.

This cocrystallization is confirmed by the ΔH_L^{n-sc} values larger than the melting enthalpy of neat LLDPE, which indicates that the cocrystallized wax melted together with the LLDPE in the blends. Cocrystallization refers to the short straight wax chains crystallizing with the folded LLDPE chains in the same lamellae. The other wax chains that did not cocrystallize with the LLDPE chains, crystallized

separately in the amorphous phase of the LLDPE. The cocrystallized wax will melt at the same temperature as the LLDPE, while the separately crystallized wax will melt at a lower temperature. It is further interesting that the ΔH_w^{n-sc} values generally increased with increasing wax fraction in the blend, indicating that a smaller percentage of the wax in the blend cocrystallized with the decreasing LLDPE fraction.

Another important observation was that no wax melting peak was observed at wax fractions smaller than 10 wt.% (Fig. 4). In contrast, the normalised melting enthalpy of the LLDPE fraction was observably higher than the melting enthalpy of neat LLDPE. This observation indicates that all the wax in the blend has probably cocrystallized with the LLDPE, increasing the amount of crystalline material melting at this temperature.

The difference between the melting enthalpy values of neat wax for slow and fast cooling is less than 1%, as observed in Table 3. There are also no significant differences

Table 3 Melting enthalpies of the LLDPE, wax, and the blends cooled under different conditions

	M3 wax melting enthalpies [J g^{-1}]				LLDPE melting enthalpies [J g^{-1}]			
	ΔH_w^{ob-sc}	ΔH_w^{n-sc}	ΔH_w^{ob-qc}	ΔH_w^{n-qc}	ΔH_L^{ob-sc}	ΔH_L^{n-sc}	ΔH_L^{ob-qc}	ΔH_L^{n-qc}
Neat wax	154.5 ± 5.7		153.2 ± 7.3					
Neat LLDPE					69.5 ± 0.1		71.7 ± 9.9	
95/5 w/w LLDPE/wax					71.3 ± 1.8	75.1	68.2 ± 1.2	71.8
90/10 w/w LLDPE/wax	4.2 ± 0.9	42.0	4.6 ± 1.0	46	71.3 ± 6.3	79.2	72.6 ± 6.0	80.7
80/20 w/w LLDPE/wax	10.2 ± 0.4	51.0	10.3 ± 2.4	51.5	69.3 ± 5.2	86.6	77.0 ± 12.2	96.3
70/30 w/w LLDPE/wax	22.4 ± 1.3	74.7	20.2 ± 0.6	67.3	64.2 ± 3.9	91.7	67.9 ± 4.4	97.0
60/40 w/w LLDPE/wax	45.0 ± 1.0	112.5	36.3 ± 3.6	90.8	52.3 ± 1.4	87.2	45.0 ± 3.2	75.0

sc slow-cooled, qc quench-cooled, ob observed enthalpy, n normalised enthalpy, w wax, L LLDPE

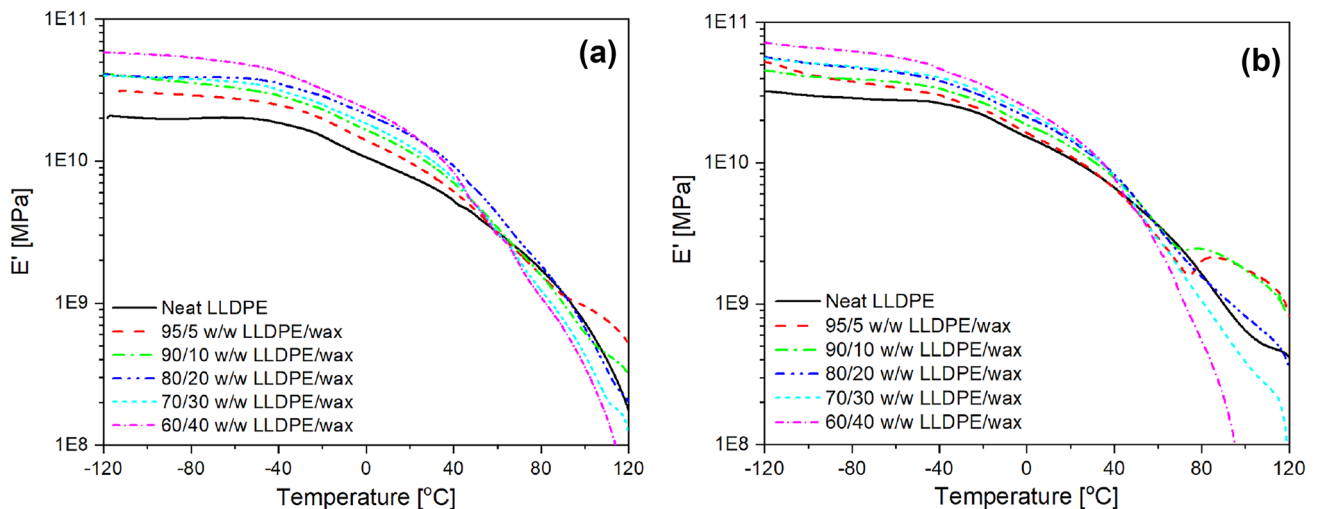


Fig. 5 Storage modulus as a function of temperature for (a) slow-cooled and (b) quench-cooled neat LLDPE and various LLDPE/wax blends

between the melting enthalpies of the wax in the fast- and slow-cooled blends. Therefore, it is clear that supercooling of the wax and LLDPE/wax blends in liquid nitrogen did not affect the wax crystallinity. Wax chains are short compared to most polymer chains and crystallize with straight chains instead of folding to form crystalline lamellae [49]. A similar increase in the melting enthalpy of the slow- and quench-cooled samples as the wax content in the blends was increased (Table 3), shows that the wax also cocrystallized with the LLDPE when the blends were cooled in liquid nitrogen. Although the high cooling rate was reported to affect the size of the crystals, it seems not to prohibit wax crystallization or reduce the wax crystallinity [50, 51].

There was also no significant difference between the melting enthalpies of LLDPE in the blends cooled through quenching in liquid nitrogen and those cooled at room

temperature. LLDPE, like other polyethylenes, crystallizes so fast that even the presence of wax or fast cooling at liquid nitrogen temperatures could not change its crystallization behaviour [15, 51]. The flexible polyethylene chains above its glass transition and the simple chemical repeat unit are responsible for this fast crystallization [52].

Thermomechanical properties of LLDPE/wax blends

Figure 5 shows the storage modulus of the slow- and quench-cooled neat LLDPE and LLDPE/wax blends as a function of temperature. In Fig. 5a, b, it is clear that an increase in wax content generally increased the modulus of the different blends. A fraction of wax crystals would have crystallized in the amorphous parts of the LLDPE or between the lamellar stacks. Van der Waals bonds between the wax crystals

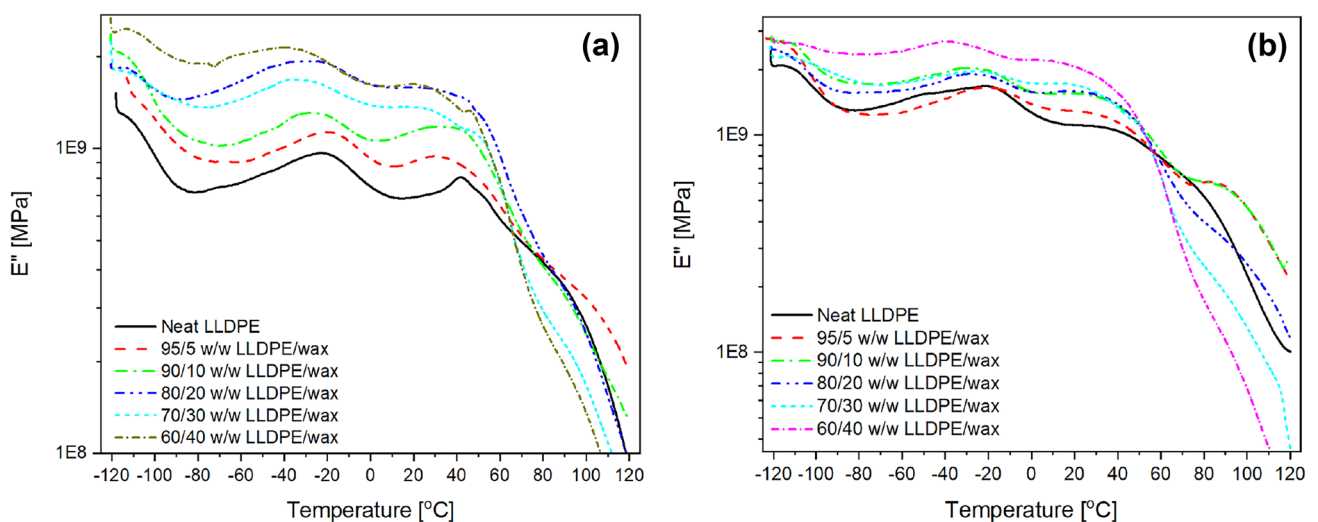


Fig. 6 Loss modulus as a function of the temperature of (a) slow-cooled and (b) quench-cooled neat LLDPE and various LLDPE/wax blends

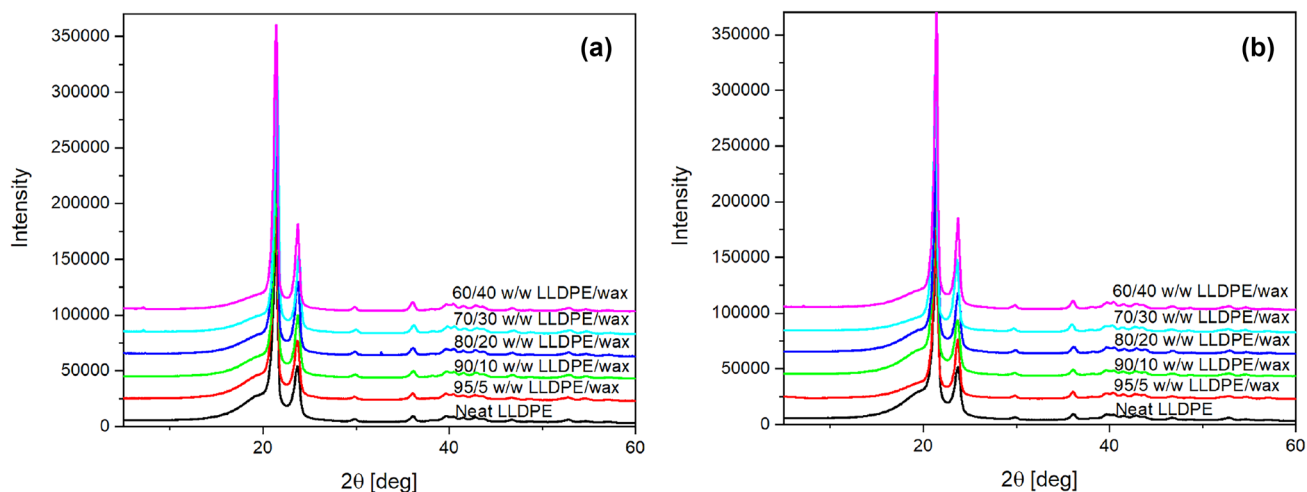


Fig. 7 X-ray diffraction spectra of (a) slow-cooled and (b) quench-cooled neat LLDPE and LLDPE/wax blends

and the LLDPE chains would have decreased the chains' mobility and increased the sample stiffness. The presence of wax crystals also increased the total crystallinity of the blends beyond that of neat LLDPE. It is known that higher crystallinities increase sample stiffness. The increased crystallinities of these samples can be seen in the increased total enthalpy of the blends compared to that of neat LLDPE (Table 3).

Three relaxation peaks were observed for LLDPE and the blends (Fig. 6). The peak at about -110 °C is called the γ -transition and is regarded by some authors as the glass transition [53]. The transition is related to motions of the backbone CH_2 units in the amorphous and crystalline region of LLDPE. It is also defined as crankshaft movements of the amorphous parts with higher free volume than the crystalline region. It was found that the slow-cooled samples had larger crystal lamellae and a larger crystalline fraction than the quench-cooled samples. The temperature difference was explained by the significant contribution from the crystalline fraction [54]. The peak that appears between -20 and -40 °C is called the β -transition, which is absent in a highly crystalline high-density polyethylene (HDPE) because this polymer has very few chain branches [21]. According to

some authors, the β -transition is attributed to a transition at the branch points on the chains of LLDPE. However, other authors relate it to the glass transition [20, 21].

The peak and peak shoulder observed in Fig. 6 between 40 and 60 °C are due to the α - and α' -transitions, respectively. These transitions are much more obvious in the slow-cooled samples, and are linked to the movement of the amorphous chains between crystals and lamellar slippage within crystals. This transition gradually disappeared with increasing wax content. Since the wax is not yet molten between 40 and 60 °C, it cannot create more free volume. However, as already mentioned, the wax crystals acted as physical crosslinks and as such, they immobilized the interlamellar amorphous material, which inhibited the transition in this temperature range [55, 56]. In the quench-cooled samples, this transition is weak for neat LLDPE and almost invisible for the blend samples. It could be that, although the faster cooling did not significantly change the total crystallinity of LLDPE, it gave rise to the formation of smaller crystals and less interlamellar amorphous material. However, as in the case of the slow-cooled blend samples, the wax crystals in the interlamellar amorphous LLDPE acted as physical

Table 4 The X-ray diffraction peak intensities of the LLDPE and blends cooled under different conditions

Sample	Slow-cooled samples		Quench-cooled samples	
	Peak intensity ($2\theta \approx 21^\circ$)	Peak intensity ($2\theta \approx 24^\circ$)	Peak intensity ($2\theta \approx 24^\circ$)	Peak intensity ($2\theta \approx 24^\circ$)
Neat LLDE	172563	54262	170066	51707
95/5 w/w LLDPE/wax	184765	57218	174568	56613
90/10 w/w LLDPE/wax	189257	59748	178782	53822
80/20 w/w LLDPE/wax	224519	70553	191221	58325
70/30 w/w LLDPE/wax	234025	72942	238448	67838
60/40 w/w LLDPE/wax	260349	81720	273132	85184

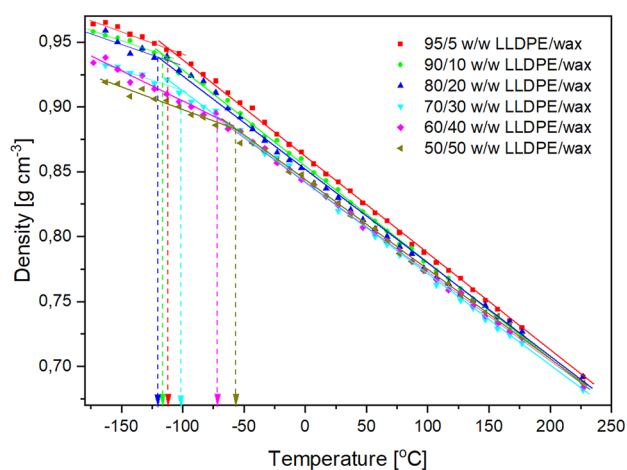


Fig. 8 Average density of short-chain LLDPE/wax blend models cooled step-wise in NPT-MD simulations as a function of temperature

crosslinks which caused the disappearance of the peak between 40 and 60 °C.

X-ray diffraction analysis

Figure 7 shows the X-ray diffraction (XRD) spectra of neat LLDPE and the blends. The spectra show that the samples were semi-crystalline, with sharp crystalline peaks and an amorphous halo visible below the two most intense peaks. The two most intense crystalline peaks around $2\theta = 21^\circ$ and 24° correspond to the (110) and (200) lattice planes of an orthorhombic crystal structure [9]. No new peaks are visible for the LLDPE/wax blends since the LLDPE and wax have the same crystal structure, as seen from XRD spectra obtained for a paraffin wax [57].

The increasing wax content in the LLDPE/wax blends increased the peak intensity (Table 4). This increased peak

intensity confirms the DSC results of an increase in the total crystallinity of the samples with increasing wax content, which confirms the cocrystallization of some of the wax with the LLDPE. As is the case with the DSC results, there are no significant differences between the XRD results of the slow-cooled and quench-cooled samples, confirming the rapid crystallization of both the LLDPE and the wax.

Modeling the thermo-mechanical properties of LLDPE/wax blends

The density of short chains (100 carbons in the backbone) LLDPE mixed with the wax chains (36 carbons long) in the unit cell is plotted versus temperature in Fig. 8. All the transition temperatures determined from the curves in Fig. 8 are presented in Table 5. The transitions are labelled as either γ - or β -transitions (or relaxations), previously defined when discussing the DMA results (also see [21, 58]). When more wax (between 5 and 20%) was added to the blends, there was an increase in the γ -transition temperature. When the wax content was just above 40%, transitions were observed between -56 and -72 °C. These are known to be β -transitions for semi-crystalline polyethylene. Therefore, the results obtained from the simulations agree with those observed in the DMA analysis in terms of wax acting as a physical crosslinker in the LLDPE chains. The transition around 350 K in the neat wax models is due to the movement of the chains during melting. Some of the simulated models of the short LLDPE chains cocrystallizing with the wax are shown in Fig. 9.

The interaction of wax with long LLDPE (520 carbons in the backbone and 70 branches) chains looks different, as displayed in Fig. 10. The addition of more wax to the blends decreased the γ -transition temperature to lower values (Table 5), but a β -transition was also observed when the wax content was 20% or more (Fig. 10b) [58]. The dynamic

Table 5 Comparison between the modelled transition temperatures of LLDPE, wax and LLDPE/wax blends, and the real transition temperatures determined through DMA analysis

Sample	Modelled transition temperatures [°C]				Real DMA determined transition temperatures [°C]	
	Short LLDPE chains		Long LLDPE chains		Slow cooled samples	
	γ -transition	β -transition	γ -transition	β -transition	γ -transition	β -transition
Neat LLDPE			-87		-115	-22
95/5 w/w LLDPE/wax	-113		-94			-20
90/10 w/w LLDPE/wax	-119		-112	-40		-26
80/20 w/w LLDPE/wax	-121		-120	-62	-114	-30
70/30 w/w LLDPE/wax	-102		-128	-37	-115	-36
60/40 w/w LLDPE/wax		-72	-118	-40	-115	-40
50/50 w/w LLDPE/wax		-56				
Neat wax			-97	6		

relaxations of the LLDPE/wax blends, determined through MD simulations, correlate within 5% with the temperatures of the DMA determined γ -transitions and other published data [20, 21, 58], but the β -transition shows some fluctuations, except for the samples containing 30 and 40% wax (Table 5).

It is not expected that wax would show transitions (or relaxations) because of its highly crystalline molecular structure. However, the neat wax in Fig. 10b shows a γ -transition temperature at -97 °C, with a weak β -transition at 6 °C. The transition could have resulted from an amorphous zone between two adjacent layers of crystalline material or a linkage between two crystal layers [59]. They could also be related to a reorientation-translational motion of the

chains in Fischer–Tropsch waxes, which was observed using spin–spin relaxation measurements in nuclear magnetic resonance (NMR) [60].

Even though the total weight percentage was kept at 100% when more wax was added, the total density of the simulated blends decreased (Fig. 10b). There was a clear increase in the total volume of the blends when the LLDPE composition ratio was reduced (Fig. 11). From basic thermodynamic state equations, volume is inversely proportional to density but directly related to enthalpy. Therefore, the simulation results presented in terms of density and volume agree that the addition of wax contributed to an increase in the total crystallinity of the blends (as described in the discussion of the DSC results).

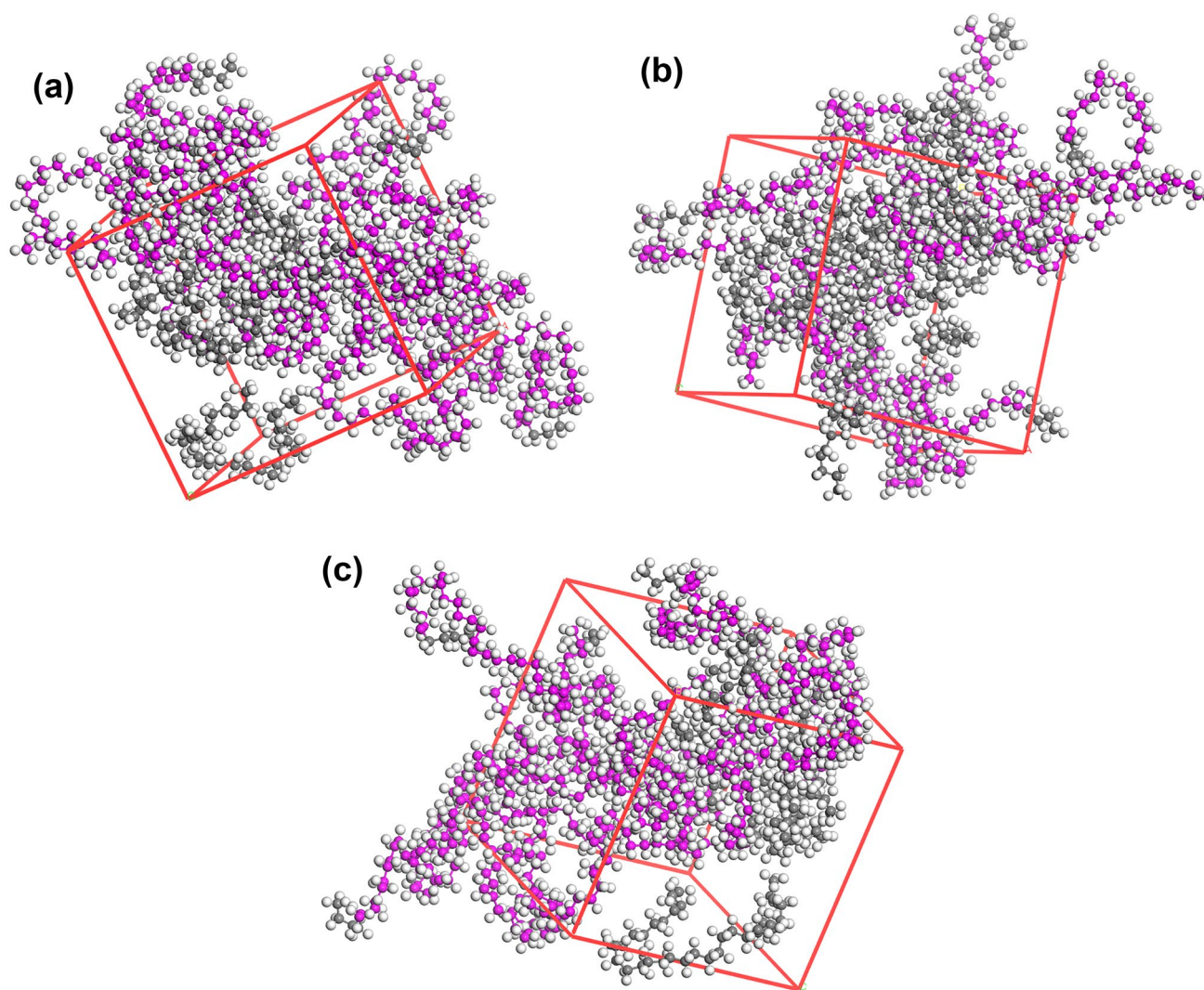


Fig. 9 **a** Amorphous cells of short LLDPE/wax (20% wax content) models at -123 °C, **b** short LLDPE/wax (40% wax content) models at -123 °C, and **(c)** short LLDPE/wax (40% wax content) models at 127 °C (in the LLDPE molecules, the purple atoms represent the

backbone carbons, the grey atoms the carbon branches, and the white atoms the hydrogens; in the wax molecules, the backbone carbons are represented by grey atoms and the hydrogens by white atoms)

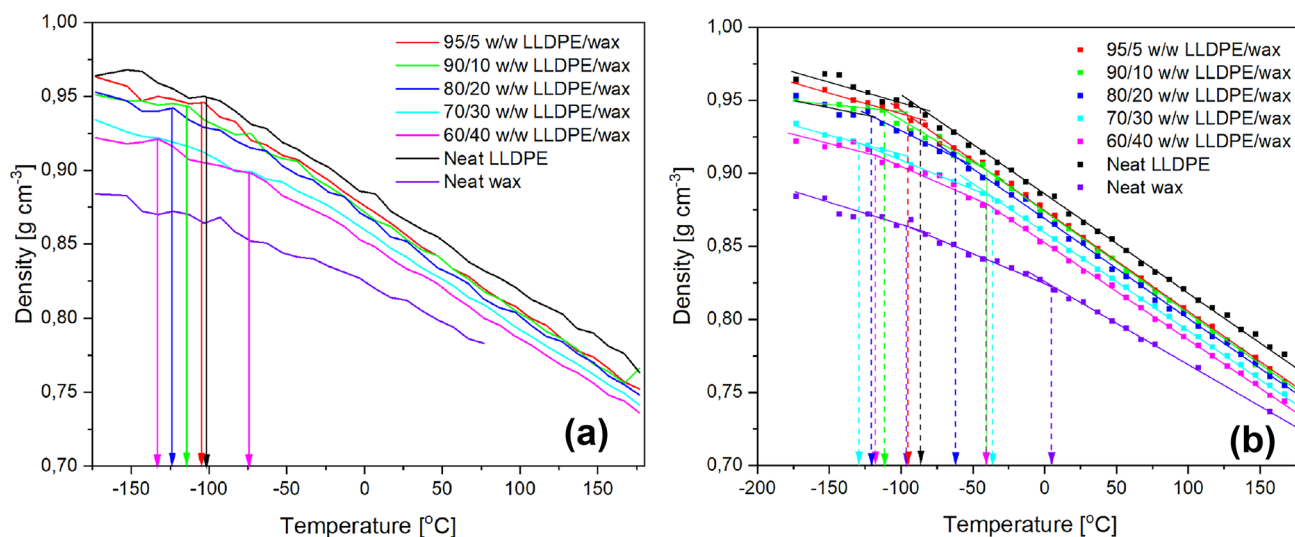


Fig. 10 Densities of long-chain LLDPE/wax blends cooled from 450 to 100 K using NPT-MD simulations: (a) Transitions estimated by observation and (b) transitions determined by the best-fitting lines

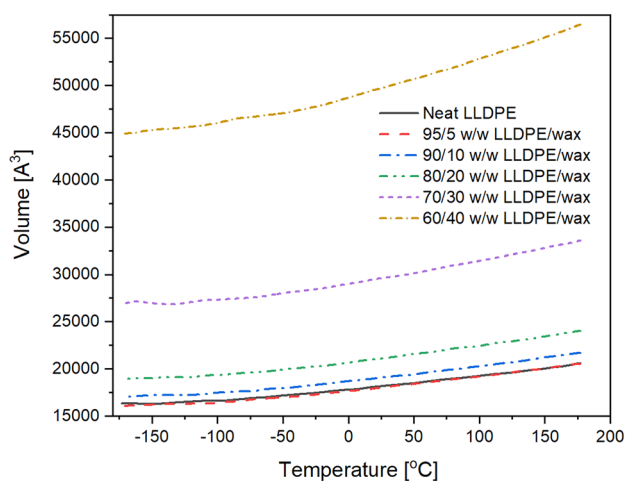


Fig. 11 Volume of long-chain LLDPE/wax blends cooled from 450 to 100 K using NPT-MD simulations

Conclusions

Cocrystallization of the components in the blends was confirmed by the small normalised melting enthalpies of wax in the blends compared to the melting enthalpy of neat wax. It was further confirmed by the ΔH_L^{n-sc} values being larger than the melting enthalpy of neat LLDPE, which proved that a certain wax fraction melted with the LLDPE in the blends. Some of the short wax chains must have crystallized separately in the amorphous parts of the LLDPE chains, acting as physical crosslinkers, which was confirmed through an increase in modulus as the wax content was increased in the blends. The cooling rate did not have an observable

effect on the overall crystallization of LLDPE, wax or the blends because both the wax and LLDPE cooled so fast that quenching in liquid nitrogen did not influence their respective crystallinities. Both DSC and XRD showed that the addition of wax increased the total crystallinity of the blends, which was also confirmed by molecular dynamic simulations in correlating enthalpy with the total volume of the blends. As observed from the experiment, our model confirmed that some wax chains were cocrystallized with the LLDPE lamellar stacks.

Acknowledgements The University of the Free State is acknowledged for financial support through the Postgraduate School, and for providing computer hardware resources. The Centre for High Performance Computing, and North-West University – High Performance Computing, are acknowledged for providing all the software resources used in the project.

Funding Open Access funding provided by the Qatar National Library.

Declarations

Conflict of interest All the authors confirm that they have no financial or commercial conflict of interest.

Open Access This article is licensed under a Creative Commons Attribution 4.0 International License, which permits use, sharing, adaptation, distribution and reproduction in any medium or format, as long as you give appropriate credit to the original author(s) and the source, provide a link to the Creative Commons licence, and indicate if changes were made. The images or other third party material in this article are included in the article's Creative Commons licence, unless indicated otherwise in a credit line to the material. If material is not included in the article's Creative Commons licence and your intended use is not permitted by statutory regulation or exceeds the permitted use, you will

need to obtain permission directly from the copyright holder. To view a copy of this licence, visit <http://creativecommons.org/licenses/by/4.0/>.

References

1. Abu-Sharkh BF, Giri AM, Hussein IA (2004) Influence of branch content on the microstructure of blends of linear and octene-branched polyethylene: A MD simulation study. *Eur Polym J* 40:1177–1182
2. Ramos J, Vega JF, Martínez-Salazar J (2015) A molecular dynamics study of the effects of branching characteristics of LDPE on its miscibility with HDPE. *Macromolecules* 48:5016–1502
3. Lin L, Argon AS (1994) Structure and plastic deformation of polyethylene. *J Mater Sci* 29:294–323
4. Choi P (2000) Molecular dynamics studies of the thermodynamics of HDPE/butene-based LLDPE blends. *Polymer* 41:8741–8747
5. Hato MJ, Luyt AS (2007) Thermal fractionation and properties of different polyethylene/wax blends. *J Appl Polym Sci* 104:2225–2236
6. Ramos J, Vega JF, Sanmartín S, Martínez-Salazar J (2016) Coarse-grained simulations on the crystallization, melting and annealing processes of short chain branch polyolefins. *Eur Polym J* 85:5016–5027
7. Peeters M, Goderis B, Vonk C, Reynaers H, Mathot V (1997) Morphology of homogenous copolymers ethene and 1-octene. I. Influence of thermal history on morphology. *J Polym Sci B Polym Phys* 35:2689–2713
8. Piel C, Starck P, Seppälä JV, Kaminsky W (2006) Thermal and mechanical analysis of metallocene-catalyzed ethene- α -olefin copolymers: Influence of the length and number of crystallization side chains. *J Polym Sci A Polym Chem* 44:1600–1612
9. Vega JF, Jargour N, Núñez-Ramírez R, Liu G, Wang D, Trujillo M, Müller AJ, Martínez-Salazar J (2015) The influence of short chain branching on the morphology and structure of polyethylene single crystals. *J Polym Sci B Polym Phys* 53:1751–1762
10. Prathab B, Subramanian V, Aminabhavi TM (2007) Molecular dynamics simulation to investigate polymer-polymer interactions and polymer-oxide metal interactions. *Polymer* 48:409–416
11. Yamamoto T (2013) Molecular dynamics of polyethylene crystallization revisited: Crystallization from the melt and the glass in longer polyethylene. *J Chem Phys* 139:054903–054916
12. Yi P, Locker CR, Rutledge GC (2013) Molecular dynamics simulation of homogenous crystal nucleation in polyethylene. *Macromolecules* 46:4723–4733
13. Zhang X, Li Z, Lu Z, Sun C (2001) Molecular dynamics simulation of the linear low-density polyethylene crystallization. *J Chem Phys* 115:3916–3922
14. Xu J, Xu X, Chen J, Feng L, Chen W (2001) Effect of composition distribution on miscibility and co-crystallization phenomena in the blends of low density polyethylene with conventional and metallocene-based ethylene-butene copolymers. *Polymer* 42:3867–3874
15. Galante MJ, Mandelkern L, Alamo RG (1998) The crystallization of blends of different types of polyethylene: The role of crystallization conditions. *Polymer* 39:5105–5119
16. Gumedede TP, Luyt AS, Pérez-Camargo RA, Müller AJ (2017) *J Appl Polym Sci* 134:44398
17. Brucato V, Piccarolo S, La Carrubba V (2002) An experimental methodology to study polymer crystallization under processing conditions. The influence of high cooling rates. *Chem Eng Sci* 57:4129–4143
18. Martín S, Vega JF, Expósito MT, Flores A, Martínez-Salazar J (2011) A three-phase microstructural model to explain the mechanical relaxations of branched polyethylene: A DSC, WAXD and DMTA combined study. *Coll Polym Sci* 289:257–268
19. Laredo E, Suarez N, Bell A, Rojas de Gáscue B, Gomez MA, Fatou JMG (1999) α , β and γ relaxations of functionalized HD polyethylene: A TSDC and a mechanical study. *Polymer* 40:6405–6416
20. Alberola N, Cavaille JY, Perez J (1992) Mechanical γ and β relaxations in polyethylene - II. Physical models of the mechanical γ relaxation in polyethylene. *Eur Polym J* 28:949–953
21. Simanke AG, Galland GB, Freitas L, da Jornada JAH, Quijada R, Mauler RS (1999) Influence of the comonomer content on the thermal and dynamic mechanical properties of metallocene ethylene/1-octene copolymers. *Polymer* 40:5489–5495
22. Klein J, Ball R (1979) Kinetic and topological limits on melt crystallisation in polyethylene. *Faraday Discuss Chem Soc* 68:198–209
23. DiMarzio EA, Guttman CM, Hoffman JD (1979) Is crystallization from the melt controlled by melt viscosity and entanglement effects? *Faraday Discuss Chem Soc* 68:210–217
24. Wingall GD, Alamo RG, Londono JD, Mandelkern L, Stehling FC (1996) Small-angle neutron scattering investigations of liquid-liquid phase separation in heterogeneous linear low-density polyethylene. *Macromolecules* 29:5332–5335
25. Fan ZJ, Williams MC, Choi P (2002) A molecular dynamics study of the effects of branching characteristics of LDPE on its miscibility with HDPE. *Polymer* 43:1497–1502
26. Zhang X, Li Z, Lu Z, Sun C (2002) Roles of branch content and branch length in copolyethylene crystallization: Molecular dynamics simulations. *Macromolecules* 35:106–111
27. Van Krevelen DW, Te Nijenhuis K (2009) *Properties of Polymers*. Elsevier Science, Amsterdam
28. Otegui J, Vega JF, Martín S, Crus V, Flores A, Domingo C, Martínez-Salazar J (2007) The unit cell expansion of branched polyethylene as detected by Raman spectroscopy: An experimental and simulation approach. *J Mater Sci* 42:1046–1049
29. Gumedede TP, Luyt AS, Pérez-Camargo RA, Iturrospe A, Arbe A, Zubitur M, Mugica A, Müller AJ (2016) Plasticization and co-crystallization in LLDPE/wax blends. *J Polym Sci B Polym Phys* 54:1469–1482
30. Wang J, Zhu X, Lu X, Zhou Z, Wang G (2015) On structures and properties of polyethylene during heating and cooling processes based on molecular dynamics simulations. *Comput Theor Chem* 1052:26–34
31. Cai T, Ma Y, Yin P, Hu W (2008) Understanding the growth rates of polymer cocrystallization in the binary mixtures of different chain lengths. *J Phys Chem B* 112:7370–7376
32. Jiang X, Li T, Hu W (2015) Understanding the growth rates of polymer cocrystallization in the binary mixtures of different chain lengths: Revisited. *J Phys Chem B* 119:9975–9981
33. Luo Z, Jiang J (2010) Molecular dynamics and dissipative particle dynamics simulations for the miscibility of poly(ethylene oxide)/poly(vinyl chloride) blends. *Polymer* 51:291–299
34. Glova AD, Falkovich SG, Dmitrienko DI, Lyulin AV, Larin SV, Nazarychev VM, Karttunen M, Lyulin SV (2018) Scale-dependent miscibility of polylactide and polyhydroxybutyrate: Molecular dynamics simulations. *Macromolecules* 51:552–563
35. <http://accelrys.com/products/collaborative-science/biovia-materials-studio>. Accessed 29 Sep 16
36. <https://www.chpc.ac.za>. Accessed 02 Aug 21
37. <http://accelrys.com/products/collaborative-science/biovia-materials-studio/references/dmol3-references/dmol3-2016.html>. Accessed 29 Sep 16
38. Burke K (2012) Perspective on density functional theory. *J Chem Phys* 136:150901–150909
39. Hincliff A (2008) *Chemical modelling: Application and theory*. The Royal Society of Chemistry, Cambridge

40. Perdew JP, Burke K, Wang Y (1996) Generalized gradient approximation for the exchange-correlation hole of a many-electron system. *Phys Rev B* 54:16533–16539
41. Henry DJ, Varano A, Yarovsky I (2008) Performance of numerical basis set DFT for aluminium clusters. *J Phys Chem A* 112:9835–9844
42. Jang SS, Jang YH, Kim Y, Goddard WA, Flood AH, Laursen BW, Tseng H, Stoddart JF, Jeppesen JO, Choi JW, Steuerman DW, Delonno E, Heath JR (2005) Structures and properties of self-assembled monolayers of bistable [2] rotaxanes on Au (111) surfaces from molecular dynamics simulations validated with experiment. *J Amer Chem Soc* 127:1563–1575
43. Doran M, Choi P (2001) Molecular dynamics studies of the effects of branching characteristics on the crystalline structure of polyethylene. *J Chem Phys* 115:2827–2830
44. Sun H, Ren P, Fried JR (1998) The COMPASS force field: Parameterization and validation for phosphazenes. *Comput Theor Polym Sci* 8:229–246
45. Sun H, Jin Z, Yang C, Akkermans RLC, Robertson SH, Spenley NA, Miller S, Todd SM (2016) COMPASS II: Extended coverage for polymer and drug-like molecule databases. *J Mol Model* 22:47
46. Sun H (1998) COMPASS: An ab initio force-field optimised for condensed-phase applications: Overview with details on alkane and benzene compounds. *J Phys Chem B* 102:7338–7364
47. Theodorou DN, Suter UW (1986) Atomistic modeling of mechanical properties of polymeric glasses. *Macromolecules* 19:139–154
48. Fu Y, Liao L, Lan Y, Yang L, Mei L, Liu Y, Hu S (2012) Molecular dynamics and mesoscopic dynamics simulations for prediction of miscibility in polypropylene/polyamide-11 blends. *J Mol Struct* 1012:113–118
49. Bower DI (2002) An introduction to polymer physics. Cambridge University Press, Cambridge
50. Webber RM (1999) Low temperature rheology of lubricating mineral oils: Effects of cooling rate and wax crystallization on flow properties of base oils. *J Rheol* 43:911–931
51. Zhuruvlev E, Madhavi V, Lustiger A, Androsch R, Schick C (2016) Crystallization of polyethylene at large undercooling. *ACS Macro Lett* 5:365–370
52. Willbourn AH (1958) The glass transition in polymers with the $(\text{CH}_2)_n$ group. *Trans Faraday Soc* 54:717–729
53. Khonakdar HA, Wagenknecht U, Jafari SH, Hässler R, Eslami H (2004) Dynamic mechanical properties and morphology of polyethylene/ethylene vinyl acetate copolymer blends. *Adv Polym Techn* 23:307–315
54. Matthews RG, Unwin AP, Ward IM, Capaccio GJ (1999) A comparison of the dynamic mechanical relaxation behavior of linear low- and high-density polyethylenes. *Macromol Sci B Phys* 38:123–143
55. Bartczak Z, Vozniak A (2019) WAXS/SAXS study of plastic deformation instabilities and lamellae fragmentation in polyethylene. *Polymer* 177:160–177
56. Bartczak Z (2018) Evaluation of effective density of the molecular network and concentration of the stress transmitters in amorphous layers of semicrystalline polyethylene. *Polym Testing* 68:261–269
57. Li Y, Samad YA, Polychronopoulou K, Alhassan SM, Liao K (2014) From biomass to high performance solar-thermal and electric-thermal energy conversion and storage materials. *J Mat Chem* 2:7759–7765
58. Borah JS, Chaki TK (2011) Dynamic mechanical, thermal, physico-mechanical and morphological properties of LLDPE/EMA blends. *J Polym Res* 18:569–578
59. Reynhardt EC, Riederer M (1994) Structures and molecular dynamics of plant waxes. *Eur Biophys J* 23:59–70
60. Basson I, Reynhardt EC (1988) An investigation of the structures and molecular dynamics of natural waxes. II. Carnauba wax. *J Phys D Appl Phys* 21:1429–1433

Publisher's note Springer Nature remains neutral with regard to jurisdictional claims in published maps and institutional affiliations.